Mössbauer Spectroscopy and Neutron Scattering: Complementary Tools for the Investigation of Magnetic Nanostructured Systems

A. Deriu, I. Bergenti, J. Moya, G. Albanese, and L. Del Bianco

Citation: AIP Conference Proceedings **765**, 171 (2005); doi: 10.1063/1.1923650
View online: https://doi.org/10.1063/1.1923650
View Table of Contents: http://aip.scitation.org/toc/apc/765/1
Published by the American Institute of Physics

Mössbauer Spectroscopy and Neutron Scattering: Complementary Tools for the Investigation of Magnetic Nanostructured Systems

A. Deriu*, I. Bergenti*, J. Moya*, G. Albanese*, and L. Del Bianco†

* *Dipartimento di Fisica and INFM, Università di Parma, Parco Area delle Scienze 7/A, 43100 Parma, Italy*
† *Dipartimento di Fisica and INFM, Università di Bologna, Viale Berti-Pichat, 40129Bologna, Italy*

Abstract. By a combined use of Mössbauer spectroscopy and polarised small angle neutron scattering, we investigated the structure and magnetic properties of iron nanoparticles obtained by inert gas condensation techniques. The detailed local information on the intrinsic magnetic properties derived from the Mössbauer data have been used in order to build up an appropriate model for the analysis of the magnetic SANS patterns; particle size distributions and magnetisation profiles have thus been deduced.

INTRODUCTION

Magnetic nanoparticles exhibit a variety of interesting physical properties that emerge as their size becomes comparable to or smaller than characteristic length scales, such as spin diffusion length, carrier mean free path or magnetic domain wall width. Experimentally interesting behaviour as giant magnetoresistance (GMR), superparamagnetism, magnetic moment enhancement and shape magnetic anisotropy have been observed depending on the particle morphology and particle environment. These peculiar effects are relevant for application in magnetic recording, sensing, and more recently in pharmacology [1-2].

In granular magnetic systems dispersed in a non-magnetic metallic matrix, magnetotransport properties have been widely investigated in past few years owing to the observation of the GMR behaviour consisting in a large variation of the electrical resistivity upon application of an external magnetic field [3]. This effect is mainly due to the spin-dependent scattering of conduction electrons at the particle-matrix interfaces or scattering from impurities. In these materials the observed GMR is strictly related to different morphological and compositional factors, such as the volume fraction of magnetic and non magnetic phases, particle shape and interfaces between magnetic and non-magnetic regions [4-6]. For this reason morphology, structure and magnetic configuration of nanoparticles needs to be known in detail in order to obtain materials tailored for specific applications. This requires the combined use of various structural and magnetic characterisation techniques. In this contest, Small Angle Neutron Scattering (SANS) and Mössbauer spectroscopy (MS) are complementary tools: SANS give information on morphology, size distribution and magnetisation profile of the particles, whereas Mössbauer spectroscopy provides detailed local information on the intrinsic magnetic properties.

In this work we report and compare results obtained by SANS and MS on of core-shell nanostructured materials prepared by the inert gas condensation (IGC) technique. In particular we focus on Fe nanoparticles surrounded by an oxide layer and on Fe-Cu intermixed nanoparticles.

THE SANSPOL TECHNIQUE

Elastic scattering of neutrons with wavelength λ at the scattering angle 2θ is associated to a momentum transfer $Q = (4\pi \sin\theta)/\lambda$. The absolute SANS intensity for a sample composed by N particles (scattering centres) per unit volume dispersed in a uniform matrix is given by [7]:

CP765, *Industrial Applications of the Mössbauer Effect,* edited by M. Gracia, J. F. Marco, and F. Plazaola

$$I \propto NF^2(Q)S(Q) \tag{1}$$

where *F(Q)* is the form factor and *S(Q)* is the inter-particle structure factor describing the interaction between them. The form factor depends on the particle shape and it is given by

$$F(Q) = \int_V d\vec{r} \exp(i\vec{Q}\cdot\vec{r})\Delta\eta = \Delta\eta V f(QR) \tag{2}$$

where V is the particle volume, R is its characteristic size, f depends only from its shape and $\Delta\eta$ is the contrast defined by the difference between the scattering length densities of the particle and the matrix. By substitution of Eq.2 in Eq.1, it can be seen immediately that the scattering intensity depends on the square of the contrast $\Delta\eta$.

Assuming non-interacting particles ($S(Q) = 1$), the scattering intensity of magnetic nanoparticles completely aligned in an external magnetic field **H** is composed by two separate factors accounting for nuclear and magnetic intensity respectively:

$$I = I_N + I_M \propto F_N^2(Q) + F_M^2(Q)\sin^2\alpha \tag{3}$$

where α is the angle between the external field and the scattering vector Q, F_N and F_M are the nuclear and magnetic form factors respectively. From the analysis of the 2D-small angle scattering pattern, one can separately deduce $F_N^2(Q)$ and $F_M^2(Q)$ and obtain thus information on the square of the contrast $\Delta\eta$ [8].

More detailed information on the magnetic structure of complex nanoparticles can be obtained using small angle scattering of polarised neutrons: the so called SANSPOL technique [9]. If we consider a beam of polarised neutrons incident on the sample with spin oriented parallel (+) or antiparallel (–) to an external magnetic field **H,** the SANS intensity contains contributions arising from both spin-flip and non spin-flip scattering processes. The scattering intensities for the two spin polarisation states are given by:

$$I^+(Q,\alpha) = F_N^2(Q) + \left(F_M^2(Q) - 2PF_N(Q)F_M(Q)\right)\sin^2\alpha \tag{4}$$

$$I^-(Q,\alpha) = F_N^2(Q) + \left(F_M^2(Q) + 2P(2\varepsilon-1)F_N(Q)F_M(Q)\right)\sin^2\alpha \tag{5}$$

where ε is the efficiency of the spin flipper device in the SANS diffractometer (see Fig. 1) and P is the polarisation degree on the neutron beam. Considering efficient spin flip and high degree of polarisation ($\varepsilon = 1$, $P = 1$), the conventional (non-polarised) SANS intensity can be expressed as the arithmetic mean of the two polarisation states:

$$I_{n\text{-}p} = \frac{1}{2}\left(I^-(Q,\alpha) + I^+(Q,\alpha)\right) \approx I_N + I_M = F_N^2(Q) + F_M^2(Q)\sin^2\alpha \tag{6}$$

The difference between the intensity of the two polarisation states gives the magnetic-nuclear cross term:

$$I^-(Q,\alpha) - I^+(Q,\alpha) = 4P\varepsilon F_N(Q)F_M(Q)\sin^2\alpha = B_{int}(Q)\sin^2\alpha \tag{7}$$

It is worth noticing that in Eq. 7 all incoherent scattering contributions are vanishing (see Ref. [9] for a detailed analysis of all the scattering contributions). Moreover the cross term $B_{int}(Q)$ is proportional to the magnetic form factor F_M. The magnetic form factor of a given particle does not interfere with the nuclear form factor of a different particle, therefore non-zero contributions to $B_{int}(Q)$ arise only from nuclear and magnetic signals of the same particle. Using the SANSPOL technique one can obtain direct information on the absolute value of the magnetic contrast with respect to the nuclear one; this can be done in terms of a γ ratio defined as

$$\gamma(Q) = \frac{B_{int}(Q)}{4F_N^2(Q)P\varepsilon} = \frac{F_M(Q)}{F_N(Q)} \tag{8}$$

If one expresses F_M and F_N according to Eq. 2 it can be easily seen [10] that γ is proportional to the ratio of the magnetic ($\Delta\eta_M$) to nuclear ($\Delta\eta_N$) contrast length density. The Q-dependence of γ provides thus useful information for the analysis of composite structures as for example magnetic core-shell particles and ferrofluids.

EXPERIMENTAL

Iron nanoparticles were obtained by the Inert Gas condensation (IGC) method [5]. High purity iron is evaporated from a heated tungsten boat in an inert Helium atmosphere. After the collisions with the inert gas, the evaporated iron atoms condensate as nanoparticles and are collected onto a cold finger. In order to generate an oxide layer surrounding the ferromagnetic iron nanoparticles, an oxygen-helium atmosphere is introduced in the evaporation chamber. After the passivation process, the core-shell particle are scraped off from the cold finger and pressed into pellets in ultra-high vacuum. Nanoparticles with an increasing mean size have been obtained by increasing the current crossing the tungsten boat, and hence the vapour temperature, during the evaporation processes. Four samples were prepared with this procedure, hereafter they are indicated as Fe-1, Fe-2, Fe-3, Fe-4.

The samples were at first characterised, from the structural point of view, by XRD. Direct evidence of the presence of a core-shell structure for the nanoparticles was then obtained from TEM measurements [5, 6].

Using a similar method a second series of Fe-Cu intermixed particles was also prepared. In this case two boats containing Fe and Cu respectively were heated and the two metals were co-evaporated at the same time. The nanoparticles were then collected on the cold finger without any additional passivation in oxygen atmosphere. Two samples of this series were prepared with different Cu/Fe volume ratios, namely $Cu_{83}Fe_{17}$, $Cu_{40}Fe_{60}$; they are indicated in the following as CuFe-1, CuFe-2. An X-ray analysis was performed also on these samples; it confirmed the presence of bcc iron and fcc copper in the expected composition ratios [11].

The SANS measurements were performed at the instrument V4 at the Hahn-Meitner-Institute in Berlin with a horizontal magnetic field of 1.1 T applied to the samples and directed perpendicular to the neutron beam. Polarised neutrons were provided by a transmission polarising cavity (Polarisation P>90%) and the polarisation was reversed using a spin flipper (efficiency $\varepsilon = 95\%$). The scattered neutrons were detected by a two-dimensional ^{3}He-detector with 64 x 64 elements of 10 x 10 mm^2. A sketch of the instrument is shown in Fig. 1. The adopted wavelength was 0.6 nm and the sample-detector distance was changed from 1.1 to 4 and 12 m exploring thus the scattering vector range $0.05<Q<3.2$ nm^{-1}. Scattering data were then corrected for sample transmission and sample holder contribution. The 2-D scattering patterns were then suitably grouped in order to deduce $B_{int}(Q)$, $F_N^2(Q)$ and $F_M^2(Q)$ according to equations (6) and (7).

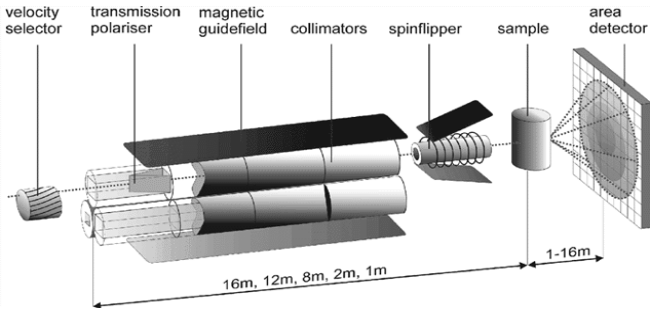

FIGURE 1. Small Angle Scattering Instrument (SANS) V4 at the HMI [12].

The Mössbauer transmission spectra were performed at room temperature using a conventional constant acceleration apparatus with a 10 mCi ^{57}Co source in Rh matrix. The data analysis was performed using the Normos Dist code [13].

RESULTS AND DISCUSSION

Core-Shell Samples

The analysis of the XRD patterns indicated the presence in all the samples of two phases that were attributed to metallic iron and to a mixture of iron oxides: magnetite (Fe_3O_4) and maghemite (γ-Fe_2O_3) (data already published [5, 6]). Mössbauer spectra for the core-shell samples are shown in Fig. 2. All the spectra show the superposition of a narrow sextet due to the iron core and of a much broader subspectrum attributable to the iron-oxide shell. The fit was

then performed in terms of a hyperfine sextet with starting parameters close to those of metallic iron (component A) and a further contribution (component B) described by a wide distribution of hyperfine fields. A quadrupole doublet of very low intensity (< 3%) had also to be added for the Fe-1 and Fe-2 spectra. The hyperfine parameters of component A are very close to each other for all the samples: the average hyperfine magnetic field turns out to be B_{HF} =33.08 ±0.08 T, a value very close to that typical for bulk α-Fe. The hyperfine field distributions resulting from the fit of component B are shown in the insets of Fig. 1. The distributions are considerably wide indicating that the oxide shell is not magnetically homogeneous. On the basis of Mössbauer measurements performed by us at low temperatures (down to 5 K, data not shown in this paper), the room temperature quadrupole doublet in spectra Fe-1 and Fe-2 can be attributed to a small fraction of fully oxidised superparamagnetic particles probably located in the outer side of the oxide-shell and/or in the interface region between nanoparticles [14].

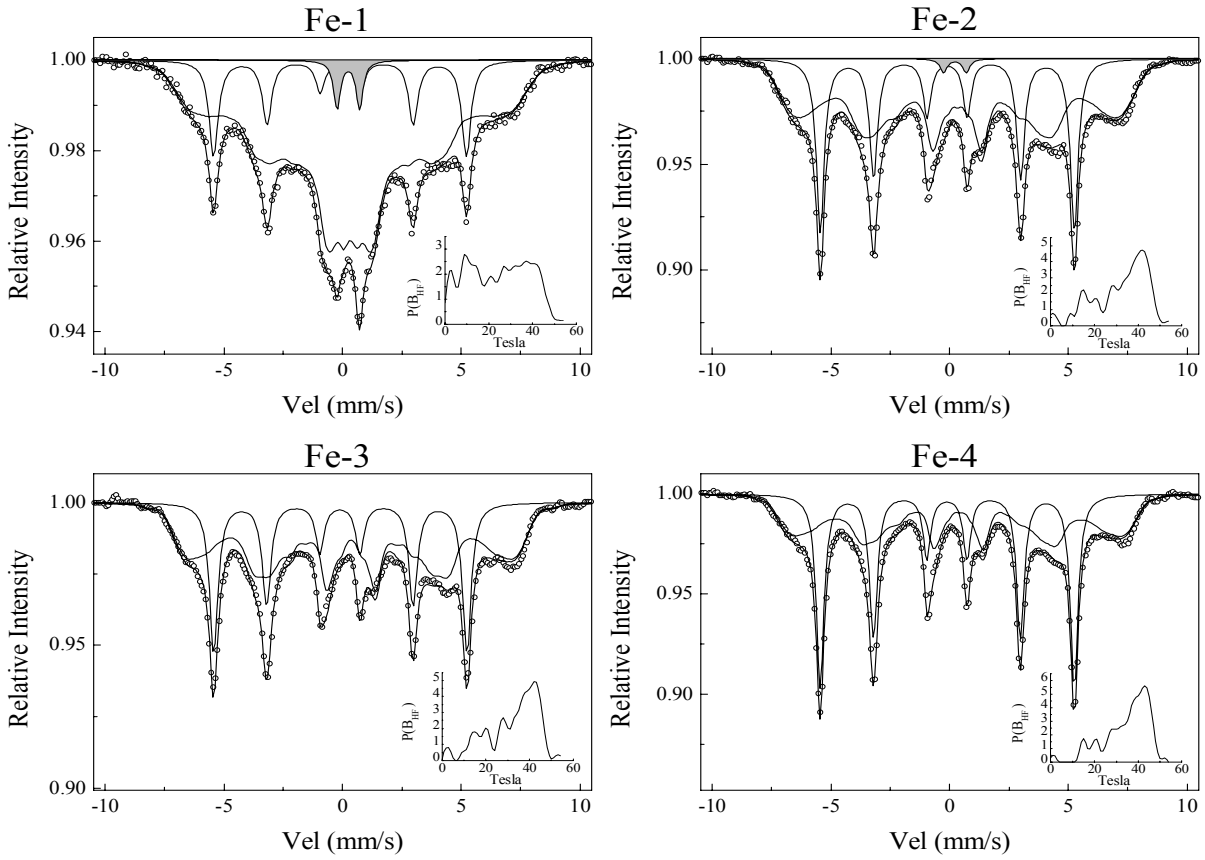

FIGURE 2. Room temperature Mössbauer spectra of the analysed core-shell samples. The subspectra due to the core and shell contributions are shown together with the total fit. The inset shows the hyperfine field distribution of the oxide subspectrum. In the spectra of samples Fe-1 and Fe-2 the small quadrupole doublets due to the superparamagnetic component (see text) are evidenced in grey.

From the areas of A and B components, assuming equal recoilless fractions and densities equal to those of bulk α-iron and iron-oxide respectively, we have deduced the relative volume of the α-Fe phase, as reported in Table I.

TABLE I.

Sample name	% Volume of the α-Fe core (Mössbauer)	Core radius (nm) (SANS)	Shell thickness(nm) (SANS)
Fe-1	9.4	2.1±0.1	2.5±0.1
Fe-2	19.5	3.3±0.1	2.4±0.1
Fe-3	18.7	3.1±0.1	2.3±0.1
Fe-4	30.4	4.7±0.1	2.3±0.1

In Fig. 3 the SANSPOL 2D patterns for the two polarizations states I^+ and I^- (Eqs. 4 and 5) are shown in the case of sample Fe-4. In the same figure the typical "butterfly" pattern of the interference term $I^-(Q,\alpha)-I^+(Q,\alpha)$ is also shown

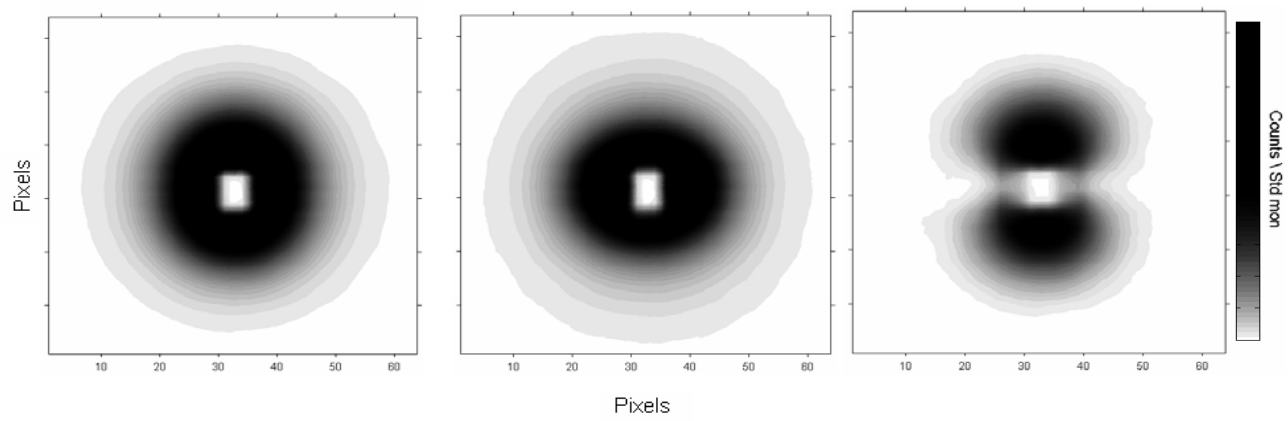

FIGURE 3. 2D SANSPOL patterns respectively for I^+, I^- *and* $I^- - I^+$ (left to right) for sample Fe-4.

The nuclear scattering intensity deduced from Eq. 6 after appropriate spatial average has been analysed in terms of a core-shell model. The scattering length profile is represented by a step-like function with a higher value for the iron core with respect to that of the oxide shell as shown in the inset in Fig. 4. Assuming spherical particles, the form factor is then [10]:

$$F(Q,r,R)=(\eta_{core}-\eta_{shell})V_r\frac{\sin(Qr)-Qr\cos(Qr)}{(Qr)^3}+(\eta_{shell})V_R\frac{\sin(QR)-QR\cos(QR)}{(QR)^3} \tag{9}$$

where r is the core radius, t is the shell thickness, and $R=r+t$ is the overall particle radius. The scattering length densities for the core and the shell are η_{core} and η_{shell} respectively. This assumption is supported by direct TEM evidence of the core-shell structure for the single nanoparticle [5, 6]. The form factor in Eq. 9 has been used in the fitting procedure assuming a log-normal distribution of particle sizes and imposing as fixed parameter the ratio between the volumes of the α-Fe phase and the oxide one as deduced from the Mössbauer results. The fitting function is then:

$$I(Q)=\frac{1}{\sqrt{2\pi e^{w^2}}X_C w}\times\int_0^\infty F^2(Q)\exp\left(\frac{1}{2}\frac{\ln(R/X_C)}{w}\right)\,dR \tag{10}$$

where X_C and w are the centroid and the width of the distribution, respectively.
The core radii and the shell thicknesses deduced from the fit are reported in Tab. I. The experimental I_N data and the result of the fit to the above model are shown in Fig. 4a for sample Fe-4.
Following the interpretation of the Mössbauer spectra we analyse the magnetic SANS intensity in terms of a contribution from the ferromagnetic iron core and a further one from a weakly magnetised oxide shell. We assume thus a non-uniform magnetic scattering length profile, η, made up from a inner region (metallic core) with constant η value (equal to $\eta_{\text{M}}^{\text{core}}$), and an outer region with a linearly decreasing scattering length $\eta_{\text{M}}^{\text{shell}}$ as shown in the inset of Fig. 4b. The form factor for magnetic scattering corresponding to the above model is given by [15].

$$F_M(Q,r,R)=(1-d)G(Qr)+d\left(\frac{R^3}{r^3}\right)G(QR)-d\left(\frac{R^3}{r^3}\right)L(QR)+d\left(\frac{R}{r}\right)L(Qr) \tag{11}$$

$d=\eta_{\text{M}}^{\text{shell}}/\eta_{\text{M}}^{\text{core}}$ is the ratio between the absolute value of the $r\to 0$ extrapolation of the shell magnetic scattering length and that of the core; $G(u)=[\sin(u)-u\cos(u)]/u^3$ represents the form factor for an homogeneous sphere, while $L(u)=[2u\sin(u)+(2-u^2)]/u^4$ is the spherical form factor for the linearly decreasing scattering length.
The fitting procedure has been carried out in a way similar to that of the nuclear contribution (Eq. 10), assuming a log-normal distribution of particle size and imposing as fixed parameter the core and shell dimensions deduced from

the analysis of the corresponding nuclear scattering intensities. The free fit parameters are therefore *d*, the centroid of the distribution X_C and its width *w*.

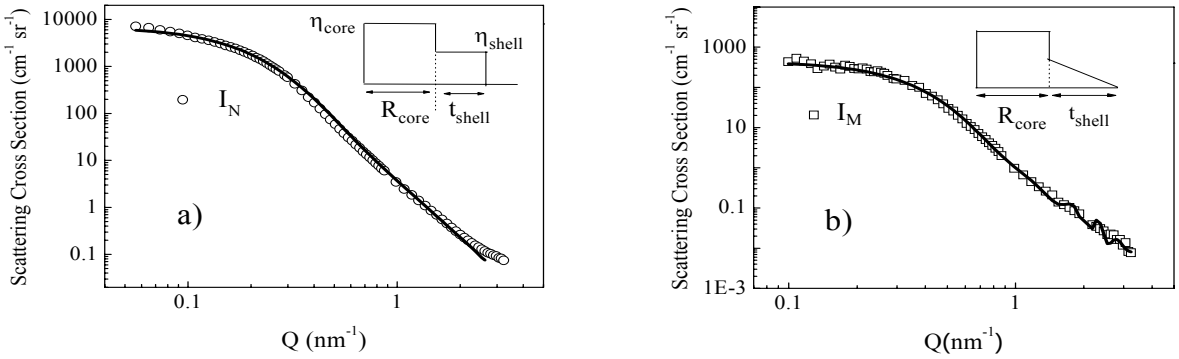

FIGURE 4. (a) Small angle nuclear scattering intensity for sample Fe-4 (open circles). The solid line is the fit to Eq. 10 assuming the scattering length profile shown in the inset. (b) Magnetic scattering intensity for Fe-4 sample (open square). The solid line is the fit to model assuming the scattering length profile shown in the inset.

In Fig. 5 we report the *Q*-dependence of the γ-ratio defined in Eq. 8. It is characterized by two changes in sign: below ~ 0.3 nm^{-1} γ is positive; it reverses its sign between the crossing points of I^+ and I^- (0.7< Q <1 nm^{-1}) and reaches a minimum at Q_{min} ~ 0.9 nm^{-1}. It becomes again positive reaching a maximum (Q_{max} ~ 1.05 nm^{-1}.) and then slowly approaches zero. As mentioned above, γ is a measure of the interference of nuclear and magnetic scattering from the same particle; we can then associate Q_{min} and Q_{max} to two characteristic length: π/Q_{min} = 3.4 nm and π/Q_{max} = 2.9 nm. They identify the average core and shell size respectively.

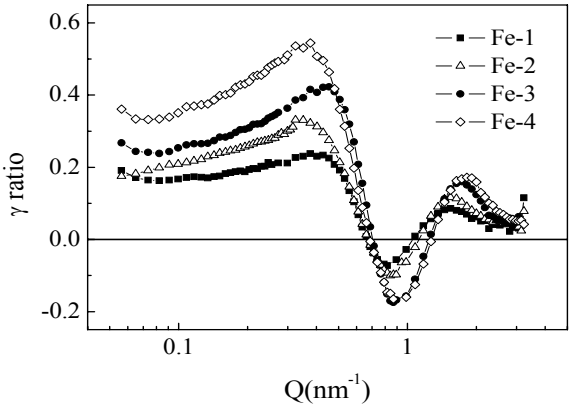

FIGURE 5. Calculated γ ratio for the measured core-shell samples

Copper and Iron Co-evaporated Nanoparticles

The SANS 2D-patterns of CuFe-1 and CuFe-2 samples are anisotropic showing the presence of magnetic contributions. In Fig. 6 the nuclear and magnetic small angle scattering intensities (a), together with the Mössbauer spectrum (b) are shown for sample CuFe-1. The nuclear scattering intensity is well fitted by a bimodal distribution of spheres that accounts for the different size of Cu and Fe particles respectively. Both distributions are quite broad (width, w = 0.4±0.1) with average radii R_1 = 2±0.3 nm and R_2 = 9.5±0.5 nm. The magnetic scattering intensity should arise from the ferromagnetic Fe nanoparticles alone. Accordingly, the magnetic intensity has been fitted by a single log-normal distribution of spheres; the resulting average particle radius is R = 1.8±0.3 nm. This model

provides a good description of the data, except for the lowest Q-region where the experimental data show a steep rise below $Q \sim 0.07$ nm^{-1} that could be associated to the presence of large magnetic iron aggregates.

The room temperature Mössbauer spectrum of sample CuFe-1 (Fig. 6b) shows a main sextet (called hereafter Sx1, with 30.2% resonant area) superimposed to a large absorption band centred near zero velocity. In addition, a further small magnetic contribution made up from two small and broad sextets (Sx2 and Sx3 with a total resonant area < 10%) must be considered. Sextet Sx1 has hyperfine parameters close to those of bulk α-Fe (isomer shift (ISO) referred to α-Fe ≈ 0, quadrupole splitting, ΔQ ≈ 0, and B_{HF}= 32.66 T). The hyperfine parameters of Sx2 and Sx3 (B_{HF}(Sx1) = 45.77 T, B_{HF} (Sx2) = 48.4 T) are typical for iron oxides, in particular they are close to those of Fe_3O_4 and γ-Fe_2O_3 [16]. The central absorption band shows a main single line centred at – 0.09 mm/s that can be ascribed to the presence of γ–Fe [17, 18]. We assign the remaining part of this central broad band to a solid solution of atomic Fe in Cu, and to a small fraction of superparamagnetic iron oxide particles. The existence of the latter contribution is confirmed by low temperature spectra (78 K) of the sample (data not shown in this paper); at room temperature it gives rise to a quadrupole doublet with ISO ≈ 0 mm/s and ΔQ = 0.33 mm/s. The solid solution of atomic Fe in Cu is described in terms of iron monomers (single paramagnetic line) and dimer aggregates (quadrupole doublet) [17]. The parameters obtained from the fit are ISO = 0.21 mm/sec for the former, and ISO = 0.17 mm/sec, ΔQ = 0.64 mm/sec for the latter.

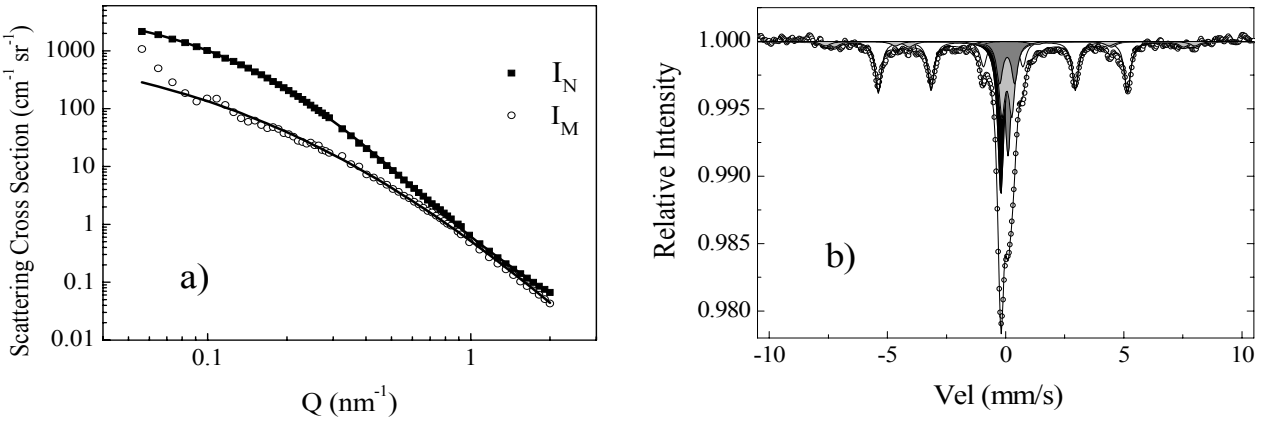

FIGURE 6 Sample CuFe-1: (a) Nuclear and magnetic scattering intensities. For the nuclear scattering curves the solid lines represent the fit to a bimodal distribution of spheres. The magnetic scattering intensity was fitted to a single distribution of spheres. (b) Mössbauer spectrum collected at 300K and the components resulting from the fit: α-Fe (white), Oxide phase (light grey), solid solution (grey), γ-Fe (black)

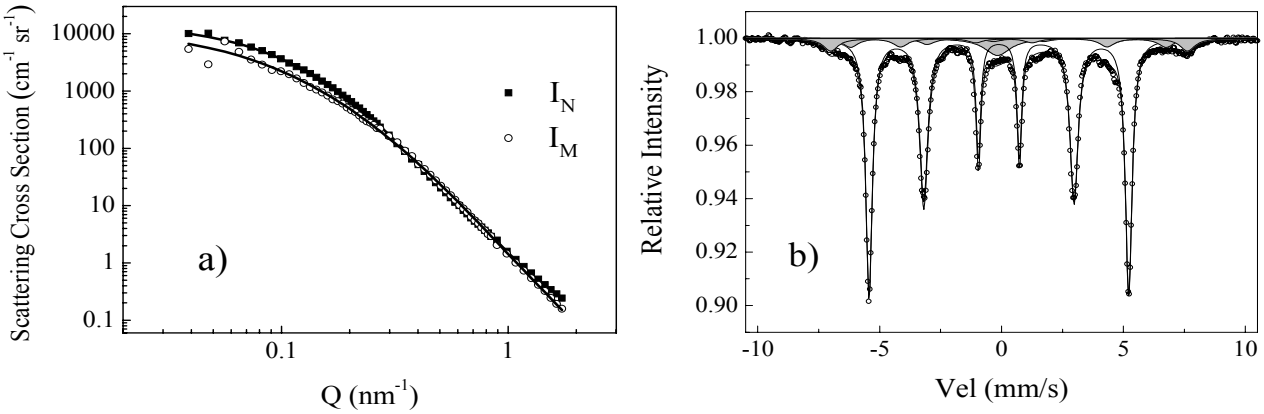

FIGURE 7 Sample CuFe-2 (a) Nuclear and magnetic scattering intensities. For the nuclear scattering curves the solid lines represent the fit to a bimodal distribution of spheres. The magnetic scattering intensity was fitted to a single distribution of spheres. (b) Mössbauer spectrum at 300K and the components obtained from the fit: α-Fe (white), oxide phases (light grey).

The same approach has been used for the interpretation of CuFe-2 data (Fig. 7). The average particle dimensions deduced from the nuclear SANS intensity are R_1 = 7.5±0.6 nm and R_2 = 16.5±0.5 nm. The magnetic scattering intensity is described by a single log normal distribution of spheres with average value R = 7.5 ±0.6 nm. The Mössbauer spectrum consist of a main sextet (80.3% resonant area) attributable to α-Fe (B_{HF} = 33 T) and two sextets (ISO = 0.60 mm/s, ΔQ = -0.42 mm/s, B_{HF} = 40.12 T; ISO = 0.31 mm/s ΔQ = 0.22 mm/s, B_{HF} = 45.34 T) and a broad single line (ISO = -0.4 mm/s, linewidth (FWHM) = 1.3 mm/s) associated to the oxide phase. Taking into account the volume ratio between the oxide phase and the α-Fe one and the average dimension of iron particles deduced by SANS, we cam estimate the oxide thickness to be around 0.5 nm.

CONCLUSIONS

The combined use of Mössbauer and SANSPOL techniques made it possible to describe in a rather detailed way the structural and magnetic features of iron nanoparticles obtain by IGC techniques. Concerning core-shell systems, information on the intrinsic magnetic properties of oxide shell and iron-core phases have been deduced, together with their relative volume ratios, from the Mössbauer spectra. These data have been used in order to build up an appropriate model for the analysis of the magnetic SANS patterns; particle size distributions and magnetisation profiles have thus been deduced. It turns out that the iron core partially polarises the oxide shell, giving rise to a magnetisation that decreases in going from the core-shell interface towards the outer particle surface.
The SANS curves of Fe-Cu co-evaporated samples show the presence of ferromagnetic Fe nanoparticles and of larger non-magnetic Cu ones. The Mössbauer spectra show in addition: i) the partial oxidation of the Fe nanoparticles that took place even without deliberate passivation during the sample preparation, ii) the presence of a solid solution of Fe in Cu in the sample with a lower iron content (FeCu-1).

ACKNOWLEDGMENTS

This work was partially supported by the Istituto Nazionale per la Fisica della Materia within the project ELTMAG (ELectronic Transport in MAgnetic Granular systems). Support from the EU through the Human Potential Programme under IHP-ARI contract HPRI-CT-1999-00020 is also acknowledged.

REFERENCES

1. Sun, S., Murray, C.B., Weller, D., Folks, L., and Moser, A., *Science* **287**, 1989 (2000).
2. Martin, J.I., Nogués, J., Liu, K., Vicent, J.L., Schuller, I.K., *J. Mag. Mag. Mat.* **256**, 449 (2003).
3. Xiao, J.Q., Jiang, J.S., Chien C.L., *Phys. Rev. Lett.* **68**, 3749 (1992).
4. Allia,P., Knobel, M., Tiberto, P., Vinai, F., *Phys. Rev. B* **52**, 15398 (1995).
5. Savini, L., Bonetti, E., Del Bianco, L., Pasquini, L., Signoretti, S., Allia, P., Coisson, M., Moya, J., Selvaggini, V., Tiberto, P., & Vinai, F., *J. Appl. Phys.* **91**, 8593 (2002).
6. Del Bianco, L. Fiorani, D. Testa A.M., Bonetti, E., Savini, L. and Signoretti, S., *Phys. Rev. B* **66**, 174418 (2002).
7. Glatter, O., and Kratky, O., Small Angle X-ray scattering, Academic Press, London (1982).
8. Wagner, W., Wiedenmann, A., Petry, W., Geibel, A., Gleiter, H., *J. Mat. Res.* **6**, 2305 (1991).
9. Heinemann, A., Wiedenmann, A., *J. Appl. Cryst.* **36**, 845 (2003).
10. Wiedenmann, A., *J. Appl. Cryst.* **33**, 428 (2000).
11. Savini, L., PhD Thesis, University of Bologna, 2003.
12. From http://www.hmi.de/bensc/instrumentation/instrumente/v4/v4-pic.html
13. R.A. Brand, Normos Program, Internal Report, Angewandte Physik, Universität Duisburg, 1987.
14. Albanese, G., Deriu, A., Moya, J., 2004. In preparation.
15. Banfi, G., Degiorgio, V., Speit, B., *J. Appl. Phys.* **74**, 6925 (1993).
16. Fujio;Y., *Jap. J. Appl. Phys.* **12**, 1850 (1973).
17. Fratzl, P., Yoshida, Y., and Vogl, G., *Phys. Rev. B* **46**, 11323 (1992).
18. Eilon, M., Ding, J., and Street, R., *J. Phys.: Condens. Matter.* **7**, 4921 (1995).